J. Fluid Mech. (2002), *vol.* 453, *pp.* 239–261.
DOI: 10.1017/S0022112001006899 Printed in the United Kingdom

A study of three-dimensional gravity currents on a uniform slope

By ANDREW N. ROSS†, P. F. LINDEN‡ AND STUART B. DALZIEL

Department of Applied Mathematics and Theoretical Physics, University of Cambridge, Silver Street, Cambridge CB3 9EW, UK

(Received 23 March 2001 and in revised form 3 April 2001)

In many geophysical, environmental and industrial situations, a finite volume of fluid with a density different to the ambient is released on a sloping boundary. This leads to the formation of a gravity current travelling up, down and across the slope. We present novel laboratory experiments in which the dense fluid spreads both down-slope (and initially up-slope) and laterally across the slope. The position, shape and dilution of the current are determined through video and conductivity measurements for moderate slopes (5° to 20°). The entrainment coefficient for different slopes is calculated from the experimental results and is found to depend very little on the slope. The value agrees well with previously published values for entrainment into gravity currents on a horizontal surface. The experimental measurements are compared with previous shallow-water models and with a new wedge integral model developed and presented here. It is concluded that these simplified models do not capture all the significant features of the flow. In the models, the current takes the form of a wedge which travels down the slope, but the experiments show the formation of a more complicated current. It is found that the wedge integral model over-predicts the length and width of the gravity current but gives fair agreement with the measured densities in the head. The initial stages of the flow, during which time the wedge shape develops, are studied. It is found that although the influence of the slope is seen relatively quickly for moderate slopes, the time taken for the wedge to develop is much longer. The implications of these findings for safety analysis are briefly discussed.

1. Introduction

The spreading of fluids due to horizontal density gradients is important for many geophysical, environmental and industrial applications. One practical example is the dispersion of a dense gas cloud following a chemical spillage. This could be an instantaneous release of gas from the catastrophic failure of a containment vessel or a continuous release from a leaking tank. The rate of spreading, distances covered and dilution of the cloud are all important in assessing the consequence of such an accident and the risk to those living or working nearby. Other industrial applications include the movement of smoke and heat in buildings and the spreading of effluent

† Present address: School of the Environment, University of Leeds, Leeds LS2 9JT, UK. e-mail: aross@env.leeds.ac.uk

‡ Present address: Department of Mechanical and Aerospace Engineering, University of California, San Diego, 9500 Gilman Drive, La Jolla, CA 92093-0411, USA.

or cooling water from an outlet pipe. Gravity currents also occur widely in nature and include cold water running off glaciers flowing into warmer lake water, turbidity currents in the ocean and snow avalanches. Simpson (1997) describes these and other examples of gravity currents, as well as giving a good overview of the work carried out on the subject.

Gravity currents are conceptually simple but exhibit complex behaviour. In most environmental and industrial cases the flow is turbulent. Small-scale mixing processes between the ambient fluid and the current fluid, due to the turbulence, are important to the dynamics of the flow and cannot be ignored. This makes it hard to obtain simple analytic, or even numerical, solutions for the problem, even in the case of simple geometries.

Much theoretical, numerical and experimental work has been carried out on gravity currents on a horizontal surface. Experimental work by Huppert & Simpson (1980) showed that the motion could be considered as an initial slumping phase during which the current developed, followed by a self-similar phase. During the self-similar phase, the front Froude number was found to be constant. An integral model was developed to describe the stages of the flow and, considering its simplicity, provides a very good description of the bulk properties of the flow. Hallworth *et al.* (1996) carried out experiments to measure the entrainment into gravity currents and extended the integral model to include the effects of the entrainment.

However, in many real situations, the effects of topography can play an important role. Previous work by Ellison & Turner (1959) considered the motion of a continuous release in a sloping channel, forming a steady-state dense layer. They carried out laboratory experiments and found that entrainment was a function of the layer Richardson number. Britter & Linden (1980) considered the motion of a gravity current head, from a continuous source, flowing down a sloping channel. Over a large range of angles, they found that the Froude number of the head did not depend on the slope. The head increases in size through entrainment of fluid from the ambient and from flow into the head from the dense layer behind. Which of these factors is most important is found to depend on the angle of the slope.

Beghin, Hopfinger & Britter (1981) considered the motion following an instantaneous release of dense fluid in a sloping channel. By considering the gravity current as a 'thermal' they developed a model for the motion and made comparisons with experiments to determine the entrainment rate. Dade, Lister & Huppert (1994) extended the model of Beghin *et al.* (1981) for particle-laden gravity currents where the density difference is generated by small suspended particles which slowly sediment out of the current, reducing the density difference.

In a channel, the large-scale motion of the flow remains essentially two-dimensional. In contrast, for an initially circular release on a slope with no lateral boundaries, the presence of the slope means the problem loses its symmetry and is no longer axisymmetric. Previous experiments and scaling by Alavian (1986) and Tsihrintzis & Alavian (1996) have looked at the flow far from a continuous source on a slope. Bonnecaze & Lister (1999) present a shallow-water model for particle-laden currents on a slope, but no experiments have been carried out to confirm the model's assumptions or predictions. For instantaneous releases on gentle slopes, Webber, Jones & Martin (1993) and Tickle (1996) have found similarity solutions of the shallow-water equations, but there is little experimental evidence to verify these solutions. All these models are for high Reynolds numbers where the effects of viscosity are small. Lister (1992) carried out experiments on viscous gravity currents from continuous point and line sources, and presented similarity solutions for the results.

In this paper, we investigate the high-Reynolds-number flow resulting from an instantaneous release of a gravity current on an unconfined uniform slope. This situation models, for example, a catastrophic failure of a storage tank of dense gas, leading to a sudden release of a large amount of the gas. The aim of this work is to understand and predict the motion and dilution of such gravity currents. This aim is achieved through a combination of simplified theoretical models and laboratory experiments. The experiments provide data to validate both existing and new models for dense gas dispersion. They also provide insight into the detailed structure of the flow and the relative importance of different physical processes.

Catastrophic failure of a storage tank may result in the release of tens of tonnes of dense gas, corresponding to several thousand cubic metres of gas at atmospheric temperature and pressure. Many gases of interest have densities much greater than air, especially where they are stored liquefied or under pressure. The rapid expansion and change of temperature on release of the gas means that initially the thermodynamics of the gas are important. Including these thermodynamic effects adds a great deal of complexity to the problem. Assuming that these effects will only play a significant role near the source, they are neglected here. Liquefied natural gas (LNG) and chlorine have densities of $1.75\,\mathrm{kg\,m^{-3}}$ and $3.61\,\mathrm{kg\,m^{-3}}$, respectively, at atmospheric pressure and temperature, so are considerably denser than air (which has a density of $1.2\,\mathrm{kg\,m^{-3}}$), even once the initial expansion and cooling have taken place.

Only slopes with a fixed gradient are considered in this work. This is the simplest case to study first, although many situations involve far more complicated topographies. In most industrial situations, the gradient of the slope will be relatively small, perhaps no more than 10°. The slope is also likely to vary slowly compared to the depth of the gravity current. These two factors mean that in many cases the results from the present experiments are relevant.

2. Theoretical model

2.1. *The importance of a slope*

The behaviour of axisymmetric gravity currents on a horizontal surface has been well studied (see Huppert & Simpson 1980; Hallworth *et al.* 1996). When considering a current on a sloping lower boundary, it is useful to know when the slope is important. It is anticipated that it will take some time for the effect of the slope to influence the gravity current and, initially, the current will behave like a current on a horizontal surface. The position at which the effect of the slope becomes important can be estimated by looking for the stage at which the slope becomes equal to the aspect ratio of the gravity current, indicating that the change in height due to the slope is no longer insignificant compared to the height of the current. The time at which this occurs may be estimated from a integral model for an axisymmetric gravity current on a flat surface, such as that of Huppert & Simpson (1980). This model assumes that the current takes the form of a flat cylinder with radius r and height h. No entrainment occurs so the volume $V = \pi r^2 h$ is constant. The difference between the density, ρ, of the gravity current and the density, ρ_0, of the ambient fluid is included through the reduced gravity, $g' = g(\rho - \rho_0)/\rho_0$. The speed at which the front moves is controlled by the Froude number condition $\dot{r} = Fr\sqrt{g'h}$. Experimentally, it is found that the Froude number, Fr, is a constant of the flow provided the fractional depth of the gravity current head, ϕ, is less than 0.075, with a value for the constant of approximately 1.19 (see Huppert & Simpson 1980). For larger fractional depths, the

Froude number varies with ϕ. Huppert & Simpson (1980) give an empirical formula,

$$Fr = \begin{cases} \frac{1}{2}\phi^{-1/3}, & \phi > 0.075 \\ 1.19, & \phi \leqslant 0.075, \end{cases} \tag{2.1}$$

to describe the Froude number.

Taking this axisymmetric integral model and using it to find the position at which the aspect ratio of the current becomes equal to the gradient of the slope gives an estimate of when slope effects become significant. This gives a radius,

$$r_\theta = r_0 \left(\frac{h_0/r_0}{\tan\theta} \right)^{1/3}, \tag{2.2}$$

which does not depend on the value of the Froude number. For a release of small fractional depth, so the Froude number is constant, (2.2) corresponds to a time,

$$t_\theta = \frac{r_0}{2Fr\sqrt{h_0 g'}} \left[\left(\frac{h_0/r_0}{\tan\theta} \right)^{2/3} - 1 \right], \tag{2.3}$$

whereas assuming a full depth release gives a time

$$t_\theta = \frac{3r_0}{2\sqrt{h_0 g'}} \left[\left(\frac{h_0/r_0}{\tan\theta} \right)^{4/9} - 1 \right]. \tag{2.4}$$

Here, the constants r_0 and h_0 refer to the initial radius and height of the release. The angle θ gives the inclination of the slope to the horizontal. The radius r_θ also gives an estimate of the maximum up-slope extent of the gravity current. In practice, the time for which the slope is unimportant is relatively small, so the variation of the Froude number in the initial stages of the flow make only a small difference to the integral model predictions and can be neglected.

This model suggests that for any non-zero angle θ, the slope will become important after a sufficiently long time. In practice, other factors, such as viscosity, may well come into play first, meaning that the assumptions of the model break down. The time at which viscous effects become important can be estimated as

$$t \sim \left(\frac{r_0^2 h_0}{\nu g'} \right)^{1/3}, \tag{2.5}$$

which is obtained by balancing the viscous and inertial terms in the Navier–Stokes equations. Here, ν is the kinematic viscosity of the fluid. This balance suggests that for $\theta < \theta_c$, where

$$\tan\theta_c = \frac{h_0/r_0}{\left(2Fr \left[h_0^5 g' / \left(\nu^2 r_0^2 \right) \right]^{1/6} + 1 \right)^{3/2}}, \tag{2.6}$$

viscous forces dominate before there is time for the slope to become important.

For the apparatus used in the laboratory experiments discussed in § 3, (2.6) gives a critical angle of about 0.2°. If the angle of the slope is greater than θ_c, then slope effects will be significant provided $r > r_\theta$.

2.2. *A wedge integral model*

The shallow-water models of Webber *et al.* (1993) and Tickle (1996) predict a wedge-shaped similarity solution for a gravity current on a slope. In the experiments

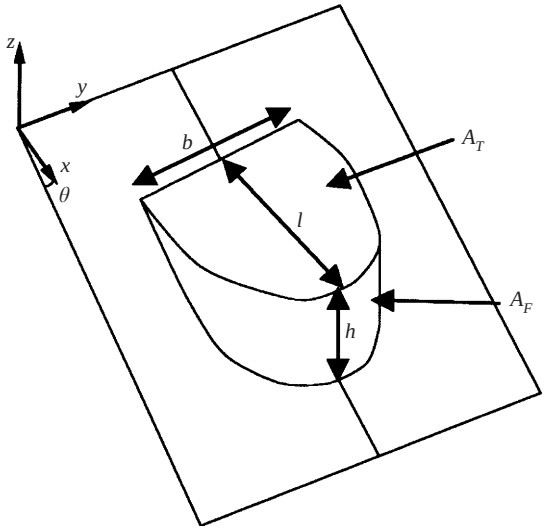

FIGURE 1. Similarity solution of the shallow water equations for a gravity current on a slope.

described in § 3, the current is observed to form a wedge moving down the slope, although the shape of the wedge is different to that predicted. Assuming that the slope is sufficiently steep and that there is time for such a wedge-shaped similarity solution to be reached, we can develop a new integral model for the motion of a gravity current on a slope. Such models are useful in clarifying the important physics in the problem and in helping to understand the experimental results. The approach is similar to that of Beghin *et al.* (1981) and Dade *et al.* (1994) for a gravity current in a sloping channel. We suppose that the current has a prescribed self-similar wedge geometry. An example of such a geometry is that predicted by Webber *et al.* (1993) and shown in figure 1 which has the front of the wedge given by the parametric equation

$$\left.\begin{aligned} x &= l\cos^2\omega \\ y &= l(\omega + \cos\omega\sin\omega) \end{aligned}\right\} \quad (-\tfrac{1}{2}\pi \leqslant \omega \leqslant \tfrac{1}{2}\pi), \tag{2.7}$$

where x and y are the down-slope and across-slope coordinates and l is the length of the wedge. The overall width and height are given by $b = \pi l$ and $h = l\tan\theta$.

The top and front areas can be written as

$$A_T = S_1 l^2, \tag{2.8}$$

$$A_F = S_2 l^2 \tan\theta, \tag{2.9}$$

respectively, and the volume by

$$V = S_3 l^3 \tan\theta. \tag{2.10}$$

The back of the wedge, where the top of the wedge meets the slope, has zero height. The values S_1, S_2 and S_3 are shape parameters describing the geometric form of the wedge. For the shape given by (2.7)

$$S_1 = \tfrac{3}{4}\pi, \quad S_2 = \tfrac{8}{3}, \quad S_3 = \tfrac{5}{16}\pi. \tag{2.11}$$

The integral model developed here is not restricted to the shape prescribed by the shallow-water model of Webber *et al.* (1993), but can be used for any self-

similar shaped wedge. Selecting different shapes leads to different values for the shape parameters (2.11).

To illustrate the differences that arise, an alternative shape with a triangular top was also used to compare with the experiments. For this shape, the shape parameters were given by

$$S_1 = 1, \quad S_2 = \sqrt{2}, \quad S_3 = \tfrac{1}{3}. \tag{2.12}$$

We make the Boussinesq approximation in deriving the new wedge integral model, i.e. the density difference is assumed to be small and can be neglected except where it multiplies the acceleration due to gravity, g. This is a good approximation for most laboratory experiments, where the density difference is created by dissolving salt in water. For dispersion of dense gases, where the density of the release may be several times greater than the density of the air, this assumption may not be valid. It does, however, lead to a significant simplification in the problem and provides a useful insight into the likely solutions. Even for initially non-Boussinesq releases, the dilution of the current by entrainment will mean that the flow will become increasingly Boussinesq. It is likely that non-Boussinesq flows will have qualitative similarities with Boussinesq flows, as was found to be the case by Gröbelbauer, Fanneløp & Britter (1993) for gravity currents on a horizontal surface.

There is also an implicit assumption that the slope is gentle enough that the flow is behaving like a gravity current and being driven by horizontal pressure differences. The shallow-water model from which the assumption of the wedge shape is made is also only valid for small slopes.

The volume of the current increases as it spreads, owing to the entrainment of ambient fluid into the denser fluid in the current. The rate of entrainment is taken as being proportional to the area over which the current is entraining multiplied by the current speed. The constant of proportionality is the entrainment coefficient, α, which is a function of the stability of the interface as measured by the layer Richardson number. From the experiments it appears that the entrainment is mainly confined to the front region of the current. We assume that the entrainment takes place over an area, A_E, near the front, of width comparable to the depth of the current, so $A_E = S_4 l^2 \tan\theta$, for some shape parameter, S_4. For the cylindrical wedge shape given by (2.7), then $S_4 = \pi\sqrt{2}$, and for the triangular wedge shape, $S_4 = 2\sqrt{2}$. An assumption like this, about the form of the entrainment, is common when modelling stratified flows, such as gravity currents and plumes.

As a result of this entrainment, the bulk mass conservation equation can be written as

$$\frac{\mathrm{d}}{\mathrm{d}t}(V) = \alpha u A_E. \tag{2.13}$$

The change in linear momentum in the down-slope direction is due to two main forces. First, there is the component of the buoyancy force acting down-slope and secondly there is a drag force associated with the motion of the current. The drag is made up of two components, the bottom drag and the form drag. The bottom drag term is given by a standard parameterization of the Reynolds stress terms for a turbulent current, $C_T u|u|A_T$, where C_T is the drag coefficient and u is the speed of the centre of mass of the gravity current. The form drag on the current takes the form $C_F u|u|A_F$. Since both A_T and A_F scale like l^2 then both of these drag terms have the same form. The likely numerical values of the drag coefficients are discussed later. It should be noted that adding a form drag of this type is equivalent to imposing a Froude number condition on the front, as done by Webber *et al.* (1993) and Tickle

(1996). We neglect variations in the speed of the current over its top resulting from the current expanding through entrainment in addition to moving down the slope. For a self-similar shape, any such variations will, at worst, make a small correction to the value of the entrainment and drag coefficients.

To take into account the ambient fluid carried along with the dense current, the mass of the current used in the momentum equation (2.14) is increased by a constant factor, $(1 + C_A)$, to give an effective 'added mass'. This is an inviscid result. The extra force is only felt while the current is accelerating. The entrained ambient fluid is at rest before it is entrained, so it imparts no momentum to the gravity current. The momentum conservation equation is therefore

$$\frac{\mathrm{d}}{\mathrm{d}t}((1 + C_A)Vu) = B \sin\theta - (C_T A_T + C_F A_F)u^2. \tag{2.14}$$

As a result of the Boussinesq approximation, the density only appears in (2.13)–(2.14) via the buoyancy $B = g'V$, and this is conserved during the flow.

The added mass coefficient, C_A, cannot easily be calculated for this wedge shape. The values for a circular cylinder and a sphere translating in irrotational potential flow are given as 1 and 0.5, respectively, by Batchelor (1967, p. 431). For a slender body of width, b, and length, l, the value is proportional to $(b/l)^2$. From this, it seems likely that the value for the wedge will be of order 1 or less.

We can look for special solutions to (2.13) and (2.14) which have a constant speed, u, corresponding to the solution of Webber *et al.* (1993). For such a solution to exist, the wedge volume must be constant, so the wedge length, l, is also constant. This means there is no entrainment. In this case, the buoyancy force is entirely balanced by the drag on the current.

To find a more general solution, we note that, provided the entrainment α is non-zero, (2.13) gives $\mathrm{d}l/\mathrm{d}t \propto u = \mathrm{d}x/\mathrm{d}t$, where x is the horizontal position of the centre of mass of the wedge shape. By a suitable choice of origin, a new horizontal coordinate x' can be defined so that $l \propto x'$. In equations (2.13) and (2.14), x' can be substituted directly for x. Using the initial conditions that $u = u_0$ and $x' = x'_0$ at $t = t_0$, and the fact that $\mathrm{d}/\mathrm{d}t = u\mathrm{d}/\mathrm{d}x'$, (2.13) and (2.14) can be integrated to give

$$l = \frac{S_4\alpha}{3S_3}x' \tag{2.15}$$

and

$$u^2 = u_\infty^2 \left(\frac{x'_0}{x'}\right)^2 + (u_0^2 - u_\infty^2)\left(\frac{x'_0}{x'}\right)^\gamma, \tag{2.16}$$

where

$$u_\infty^2 = \frac{54B\,S_3^2\cos\theta}{x_0^2\alpha^3 S_4^3(1 + C_A)(\gamma - 2)} \tag{2.17}$$

and

$$\gamma = 6\left(1 + \frac{C_T S_1 + C_F S_2 \tan\theta}{\alpha S_4 \tan\theta(1 + C_A)}\right). \tag{2.18}$$

The parameter γ controls the rate at which the speed of the current decays. Increasing the drag increases γ, causing the current to slow down more rapidly. The speed u_∞ gives the scale for the speed for large x so $u/u_\infty \sim x'_0/x'$. Both u_∞ and γ increase with increasing entrainment and added mass so the overall effect of different values of α and C_A is not immediately obvious. In the limit $\alpha \to 0$ then $x'_0 \to \infty$ in such a way

that (2.16) does not become singular, since the product $S_4\alpha x_0'/(3S_3) = l_0$ is constant. The solution is not valid in this limit. Putting $\alpha = 0$ into (2.13) and (2.14) gives an exponential form for u as a function of x'.

Writing $u = \mathrm{d}x'/\mathrm{d}t$ and substituting in (2.16) gives a differential equation for $x'(t)$. This equation cannot be integrated exactly for arbitrary values of C_T and C_F, but the solution for x can be obtained numerically.

For the no-drag case where $C_T = 0$ and $C_F = 0$, an exact solution for the centre of mass position is possible, yielding

$$x_c = \left((2u_\infty x_0' t)^2 - \frac{\left(u_0^2 - u_\infty^2\right) x_0'^6}{u_\infty^2 x_0'^2} \right)^{1/4}. \tag{2.19}$$

This predicts that for large times $x_c \sim t^{1/2}$. The same scaling is seen for large times in the entraining similarity solution of Tickle (1996).

The entrainment coefficient is found to be of order 0.1 in a variety of similar experiments (see Ellison & Turner 1959; Hallworth *et al.* 1996). Here, it is retained as a parameter to be determined experimentally to give a best fit to the data. Britter & Linden (1980) found a value of about 0.003 for the drag, C_T, for a gravity current in a smooth sloping channel. It will be greater for a rougher surface, but no experimental data is available. The form drag coefficient, C_F, is generally between 1.0 and 0.1 for most bodies. The wedge-shaped gravity current is fairly streamlined so the value is likely to be close to 0.1. Using these values for the drag coefficients and taking slopes between 5° and 20° gives values for the exponent γ between 6 and about 6.3. This is a 5% change and means that neglecting the second term in (2.18) is a reasonable approximation, i.e. drag effects are small compared to the effects of entrainment and the added mass. The exponent γ increases with decreasing slope, so for very small slopes then the drag term is relatively more important. Comparison of numerical results from this model, with and without the drag terms, shows there is little difference for the parameter values considered here. The difference between the predicted front position for $C_T = 0.01$ and $C_T = 0.0$ is less than 0.05%.

As $\theta \to 0°$ then, provided the volume of the current is constant, $A_T \to \infty$, $A_F \to 0$, $u_\infty \to 0$ and $\gamma \to \infty$. The solution is no longer physically realistic in this limit as the current will not have an infinite top and no height. This is not a contradiction as $t_\theta \to \infty$ and $r_\theta \to \infty$ as $\theta \to 0°$ so the wedge-shaped solution is never reached in this limit and the current spreads axisymmetrically for all time.

As θ increases, an angle will be reached, depending on the aspect ratio of the release, where the slope will always be important according to (2.3). As $\theta \to 90°$, then the current will become a dense thermal against a vertical wall. In this limit, the wedge shape would become very large and flat which is not appropriate. The thermal will be a more bluff shape, as discussed by Morton, Taylor & Turner (1956).

The distance, x_c, in (2.19) is the position of the centre of mass of the current. The front position is needed in order to compare with the experimental results in § 4. For the circular wedge shape given by (2.7), the centre of mass is a distance $5l/12$ from the front of the wedge so

$$x_c = x_f - \frac{5}{12} l = x_f \left(1 - \frac{5}{12} \frac{\mathrm{d}l}{\mathrm{d}x_f} \right), \tag{2.20}$$

since $x_f \propto l$. If (2.20) is substituted into (2.13) and (2.14) to change from measuring the centre of mass position, to measuring the front position, then (2.13) and (2.14) remain unchanged provided that u_∞ is divided by the factor $(1 - \frac{5}{12}(\mathrm{d}l/\mathrm{d}x_f))$ and α is

multiplied by the same factor. The effect of measuring the positions and speeds of the front rather than the centre of mass is only to alter the experimental constants and not the form of the solution. For the triangular wedge shape, the centre of mass is a distance $\frac{1}{2}l$ from the front of the wedge. For any other self-similar shape, a similar transformation will apply.

The equations of the wedge integral model were numerically integrated. As this model is only valid once sufficient time has passed for the similarity solution to develop, the simple box integral model for a gravity current on a horizontal surface, described in § 2.1, was used for the initial stages of the release. Once the current had spread out enough for front effects to be important, the circular-shaped current was transformed into a wedge-shaped current, preserving the front position, concentration and volume. Various types of integral model were used for the initial stage, both entraining and non-entraining. The results were found not to be particularly sensitive to the exact model used, since the initial stage was quite short and the spatial position at which the changeover was assumed to occur was determined by the slope, independent of the integral model used. The numerical code allowed the effect of the parameters to be studied and predictions compared with experimental results. These are discussed further in § 4.

3. Experimental set-up

Experiments were undertaken to validate the assumptions incorporated in the model described in the previous section, and test the predictions. The majority of the experiments were carried out in a tank of dimensions 2.0 m × 2.5 m × 0.85 m (width × length × depth). The tank was fitted with a false bottom that could be adjusted to give a range of slopes. Slopes in the range 5°–20° were used. A small number of experiments were also carried out in a shallower tank of internal dimensions 1.18 m × 1.49 m × 0.10 m. In this tank, slopes of up to 2.5° were possible.

A cylinder with an angled base was placed on the slope so that the top was above the water level. Salt was dissolved in the water within the cylinder to provide a density difference and red food colouring was added to aid visualization. The initial densities measured with a refractometer were from about 1.012 g cm^{-3} to 1.025 g cm^{-3}. The gravity current was released by rapidly removing the cylinder from the water. Care was taken to ensure the cylinder was lifted cleanly and with as little mixing as possible. Details of the experiments carried out are given in table 1.

The experiments were all recorded on S-VHS video using a monochrome CCD camera. This allowed later analysis with the **Dig***Image* image processing software (see Dalziel 1992). The analysis included measurements of the gravity current position, length and width as a function of time.

For some of the experiments a conductivity probe mounted on a traverse was placed in the flow. The probe was calibrated to give a reading of the salt concentration at the probe tip. The probe was connected to a PC via an analogue-to-digital converter, allowing the measurements to be logged automatically at regular intervals. This provided a means of measuring the profile and dilution of the current. A sample rate of 10 Hz was used for the experiments described here.

Previous work, such as that of Huq (1996), has shown that the fractional depth of a gravity current can be important, provided the fractional depth is not too small. Some surface current experiments were carried out in the smaller tank to confirm whether the fact the current was flowing down-slope was more important than the fact it was flowing into a deepening layer of fluid. A fresh water and dye mixture was

Exp.	θ (deg.)	g'(cm s^{-2})	V(cm^3)	Distance to probe (cm)	Length scale $V^{1/3}$(cm)	Time scale $(V^{1/3}/g')^{1/2}$ (s)
1	5	27.2	1686	—	11.9	0.66
2	5	26.85	1686	—	11.9	0.67
3	10	23.6	1847	—	12.3	0.72
4	10	23.25	1847	—	12.3	0.73
5	15	23.95	1879	—	12.3	0.72
6	15	23.95	1879	—	12.3	0.72
7	15	38.35	1686	—	11.9	0.56
8	15	10.7	1686	—	11.9	1.05
9	20	27.2	1686	—	11.9	0.66
10	20	23.25	1702	—	11.9	0.72
11	20	22.5	1718	—	12.0	0.73
12	5	25.0–29.3	1686	37.0, 54.5, 74.5, 101.0	11.9	0.64–0.69
13	10	22.1–27.2	1959	23.5, 49.5, 67.0	12.5	0.68–0.75
14	10	22.9–23.6	1767	128.5	12.1	0.72–0.73
15	10	23.25–25.0	1879	107.5	12.3	0.70–0.73
16	15	20.35–25.35	2168	49.5, 65.5	12.9	0.71–0.80
17	15	19.65–25.7	1767	51.0, 83.5	12.1	0.69–0.78
18	20	20.35–24.3	1767	37.5, 70.0, 95.0	12.1	0.71–0.77

TABLE 1. Details of initial conditions for instantaneous release gravity current experiments. The experiments were carried out in the large tank with a sloping bottom.

released into a salty ambient, causing a gravity current to flow along the surface of the water. In this case, the current was only subject to the change in fractional depth. No discernible deviation from the circular spreading shape expected for a current over a flat bottom was seen. This suggests that the slope rather than the change in fractional depth is of overriding importance. The rapid thinning of the current ensures that the fractional depth remains small, and therefore variations in the fractional depth do not significantly affect the current.

4. Experimental results

Initially, the gravity current spread in a symmetric manner similar to a current on a flat surface. The gravity current looks like a vortex ring spreading out radially from the point of release. After a short time the back (up-slope) edge became noticeably lighter than the front (down-slope) edge, showing that the back edge was thinner than the front edge. The back edge then began to move more slowly. The fluid drained from the back to the front, forming a wedge-shaped current with a thin viscous draining layer behind. This was a gradual process, making it hard to specify an exact time at which the transition to the wedge-shaped similarity solution occured.

The pictures in figure 2 were taken at times 0.5 s, 1.5 s, 2.5 s and 3.5 s after the release. The predictions of the axisymmetric integral model are superimposed. After 0.5 s, the current is still nearly axisymmetric. By 1.5 s, the effects of the slope are beginning to be seen. The current is still close to circular, but is no longer centred on the release point. The down-slope edge is also noticeably darker than the up-slope edge. The wedge shape is still not fully developed, even after 3.5 s. The actual motion in the initial stages was not as simple as the integral model suggests. The up-slope part of the current remained deeper for longer as the current did not have a horizontal top surface, as assumed, but was more nearly parallel to the bottom. It was found that

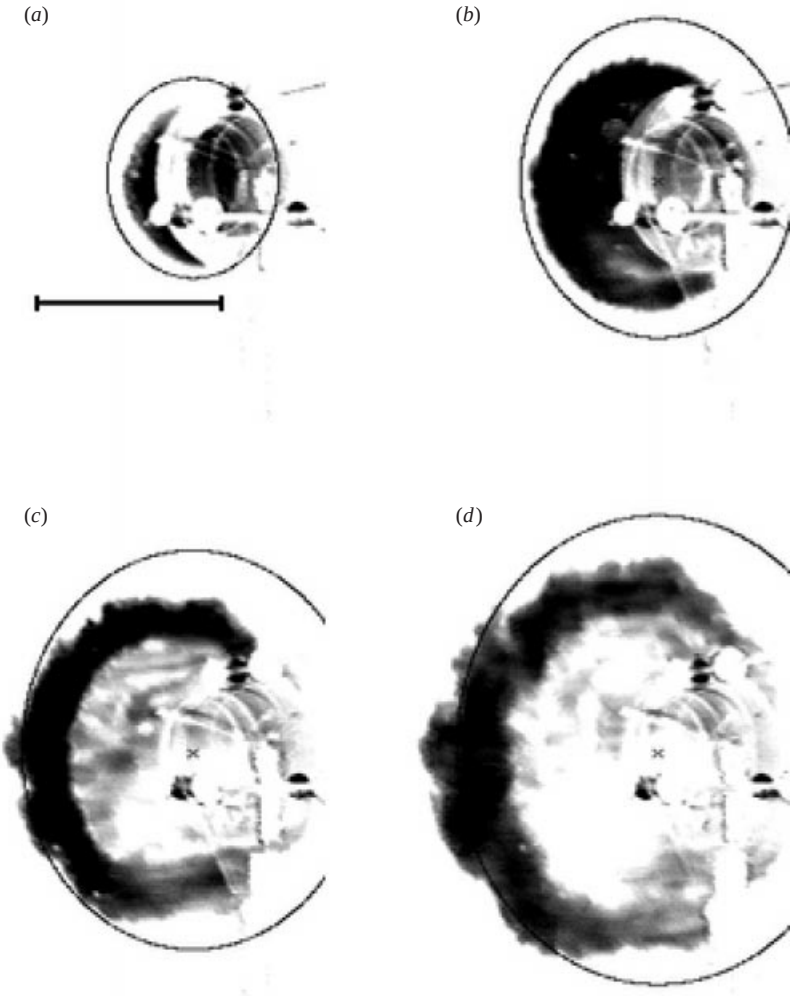

FIGURE 2. Formation of a wedge shape during experiment 5. The top of the slope is to the right-hand side of the picture and the bottom of the slope to the left. The release point shows up as the dark circle on the right of the picture. The black outline curve is the integral model prediction for this experiment. The slope is 15°. The images are at time (*a*) 0.5 s, (*b*) 1.5 s, (*c*) 2.5 s and (*d*) 3.5 s after release. The scale mark in image (*a*) is 30 cm long.

the current took longer than the estimated time to reach the wedge-shaped solution. The predicted time for the slope to become important for the experiment shown in figure 2 was 0.5 s. The current did not appear to have developed into a wedge shape until 3.5 s after the release.

For later times, the development is shown in figure 3. These pictures are at times 1.5 s, 6.5 s, 11.5 s and 16.5 s. They show the wedge shape moving down the slope. The predictions of the wedge integral model are superimposed on the figures for both the cylindrical and the triangular-shaped wedges. It can be seen that the shape of the wedge formed is more triangular than the circular shape predicted by Webber *et al.* (1993).

As light passes through the dye it is attenuated. The amount of attenuation depends on the dye concentration, which is proportional to the concentration of salt, assuming

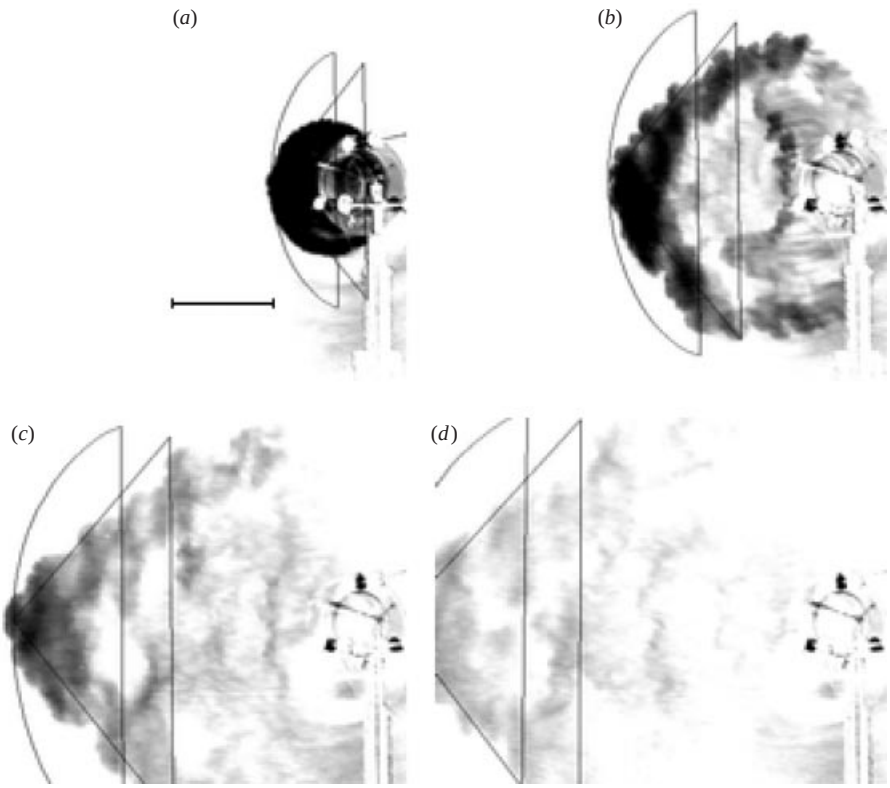

FIGURE 3. Formation of a wedge shape during experiment 5. The top of the slope is to the right-hand side of the picture and the bottom of the slope to the left. The release point shows up as the dark circle on the right of the picture. The black outline curves are the integral model predictions for this experiment with the two different assumed shapes for the wedge. The slope is 15°. The images are at time (*a*) 1.5 s, (*b*) 6.5 s, (*c*) 11.5 s and (*d*) 16.5 s after release. The scale mark in image (*a*) is 30 cm long.

the salt and dye are transported in the same way. The light intensity measured by the **Dig***Image* system therefore gave a measure of the depth integrated density, $\int g' \, \mathrm{d}z$. This can be seen qualitatively from the darkness of the current in figures 2 and 3.

As the slope was increased from 5° to 20°, it was observed that the wedge shape developed more quickly after release, as predicted by (2.3). The shape of the wedge altered to become slightly deeper and thinner as the slope increased. This is also in keeping with the integral model predictions. Only slopes up to 20° could be studied experimentally. The behaviour may be altered for larger slopes near 90°.

The data from the experiments were all non-dimensionalized with respect to the relevant length scale ($V_0^{1/3}$) and time scale $(V_0/g_0'^3)^{1/6}$. V_0 is the initial volume of the release and g_0' is the initial reduced gravity of the release. The reduced gravity, calculated from the conductivity probe measurements, was non-dimensionalized with respect to its initial value, g_0'. Figure 4 shows that the experimental data collapses well for a range of initial densities. All the densities were sufficiently small that the flow is still Boussinesq.

In order to calculate derived quantities, such as the Reynolds number and Froude number, it is necessary to know the front speed, u_f, of the gravity current. The front

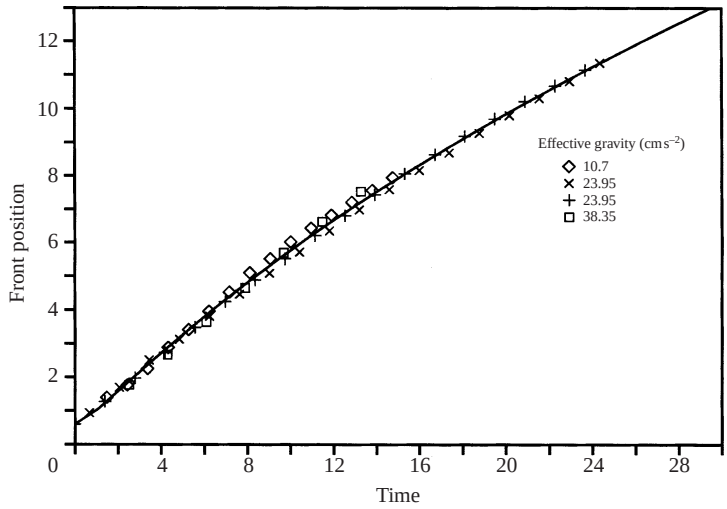

FIGURE 4. Non-dimensional down-slope position of the gravity current front against time for densities in the range 10–40 cm s^{-2}. The slope is 15° and the initial volume is constant for all the experiments (see experiments 5–8 in table 1). The solid line is the prediction from the wedge integral model. The entrainment has been chosen to provide a best fit for the data.

speed was calculated by using a least-squares method to fit a polynomial to the front position as a function of time, and then taking the first derivative of this fit to yield the speed.

From figure 5, it can be seen that the gravity current decelerates as it moves down the slope. The non-entraining shallow-water model of Webber *et al.* (1993) gives a constant speed for the current, which over-predicts the speed and front position compared to the experimental results. The entraining model of Tickle (1996) provides a slightly better fit to the front position data. The model requires the front Froude number and entrainment coefficient to be specified. The values used were those from Tickle (1996), based on experiments with dense gas. The values obtained (0.59 for the Froude number and 0.034 for the entrainment) are low compared to other values obtained for laboratory experiments with salt/fresh-water gravity currents. This may explain some of the discrepancy. The experiments were compared with the predictions of the wedge integral model using either the arc-shaped wedge given by (2.7) or the triangular-shaped wedge. This set the shape parameters S_1, S_2, S_3 and S_4 to the values given in (2.11) and (2.12), respectively. For the comparisons, the drag coefficients C_F and C_T were set to zero and the added mass coefficient was set to 1. The entrainment coefficient for each slope was determined by performing a best fit of the model predictions to the experimental front position data. The entrainment coefficient is the only free parameter varied in the model. The predictions of the two integral models for the front position are indistinguishable. This is perhaps not surprising since the entrainment coefficient was chosen to best fit the experimental front position data. The best fit values for each slope angle are given in table 2.

The variation between the lines in figure 5(*d*) illustrates the difficulty in making the experiments reproducible. Any residual motion in the dense fluid or the ambient fluid, or any slight leakage from the cylinder before release can have a significant effect on the motion of the gravity current. Great care was taken to minimize such effects.

The length and width of the gravity current are shown in figures 6 and 7. These

Slope (deg.)	Entrainment coefficient cylindrical shape	Entrainment coefficient triangular shape
5	0.3047	0.3498
10	0.1437	0.1649
15	0.1240	0.1423
20	0.1343	0.1541

TABLE 2. Details of 'best fit' entrainment coefficients for the integral model using both the cylindrical shaped wedge and the triangular-shaped wedge.

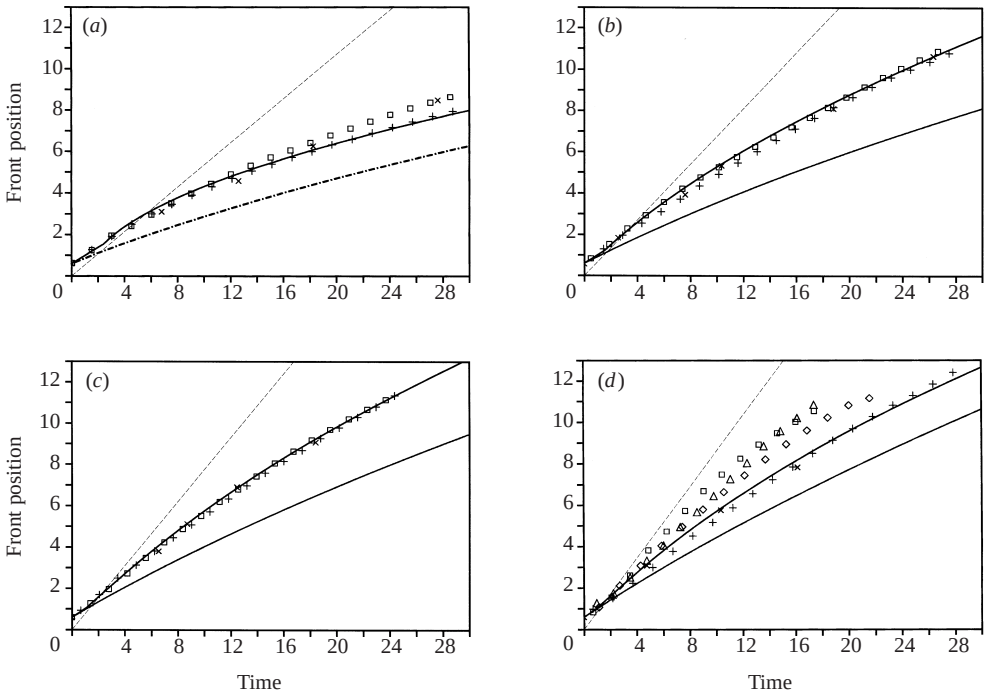

FIGURE 5. Front position of a gravity current on slopes of (*a*) 5°, (*b*) 10°, (*c*) 15° and (*d*) 20°. Each symbol represents a different experiment. —, wedge integral model developed here for the cylindrical and the triangular shapes. These are indistinguishable. - - -, non-entraining shallow-water model of Webber *et al.* (1993), –·–, entraining shallow-water model of Tickle (1996) (using the values obtained in the paper for the front Froude number and entrainment).

measurements are somewhat more subjective than the front position as the current has a thin viscous draining layer behind it, making it difficult to judge the edge. The length was measured from the front of the current to the back of the thicker front layer. The predictions of the wedge integral model for the cylindrical wedge are also shown on the graph. The wedge integral model generally seems to over-predict the current length and width. The width in particular is over-predicted. This can be seen more clearly in figure 3 where experimental images are overlaid with the outline of the model predictions. The back position is generally consistent with the experimental results, but the width is significantly less at all stages of the flow. This calls into doubt the cylindrical wedge shape in (2.7), as predicted by Webber *et al.* (1993). The triangular wedge shape gives much better agreement with the experiments. Plotting

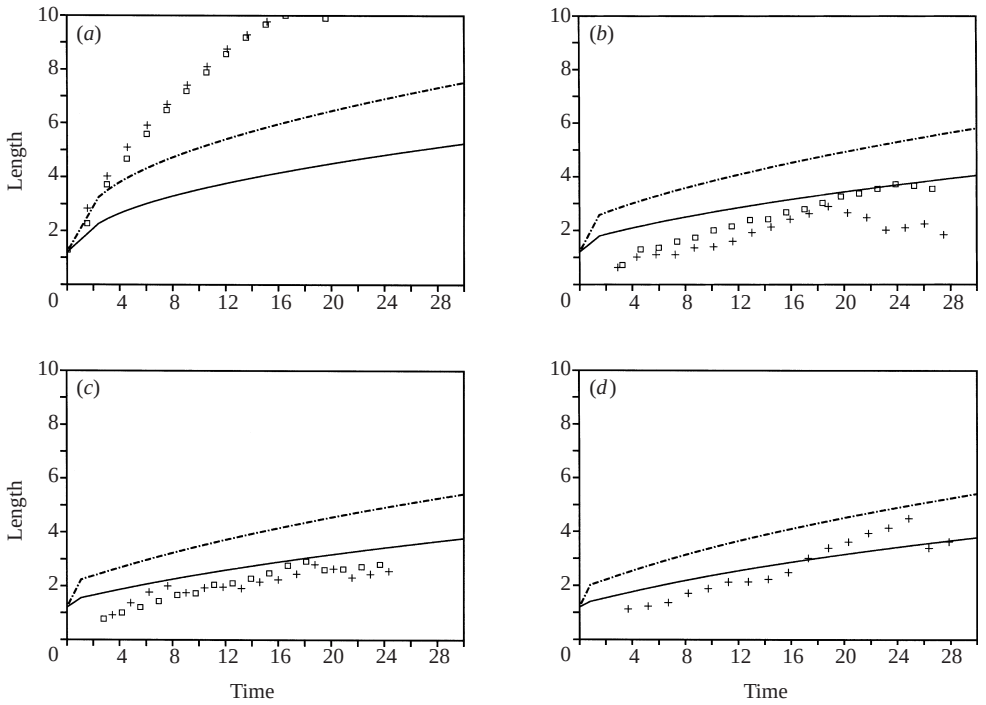

FIGURE 6. Length of the gravity current against time for slopes of (*a*) 5°, (*b*) 10°, (*c*) 15° and (*d*) 20°. +, □, experimental measurements; —, theoretical prediction of the wedge integral model in § 2 assuming the cylindrical wedge; – · –, predictions assuming the triangular wedge.

the width/length against time shows that the ratio remains nearly constant over the flow, although the value varies slightly with slope. Between 10° and 20°, the ratio is in the range of 1.5–2.0. For the slope of 5°, the ratio is significantly less than 2.0. This is due to the fact that the current did not have time to form a significant wedge shape in the tank available. The value of about 0.5 signifies that the current remained nearly circular in shape. One explanation for the wedge integral model over-predicting the size of the gravity current is that it does not take into account the fluid which is left behind the current in a thin draining layer. When the current has travelled some distance, then this may account for a significant fraction of the initial fluid. The experimental results, such as those in figure 3, suggest that the wedge shape was more pointed than rounded. The wedge with a triangular top and a width to length ratio of 2.0 was chosen to predict this shape better and also to give a better value for the width to length ratio. The results from this were compared with the results using the shape in (2.7) and with the experimental results. It was found that the two shapes gave similar predictions for the dilution of the current, however, the triangular top gave a better prediction for the gravity current plan shape. The aspect ratio for the triangle was chosen with that in mind. The predictions for both wedge shapes are shown in figures 2 and 3.

The conductivity probe measurements allowed the depth of the current to be inferred at various points down the slope. Figure 8 shows that the height of the current varies little as the current develops. Both the new wedge integral model and the model of Tickle (1996) over-predict the height of the current. A steady increase in the height is predicted, as the current entrains fluid. This does not appear to

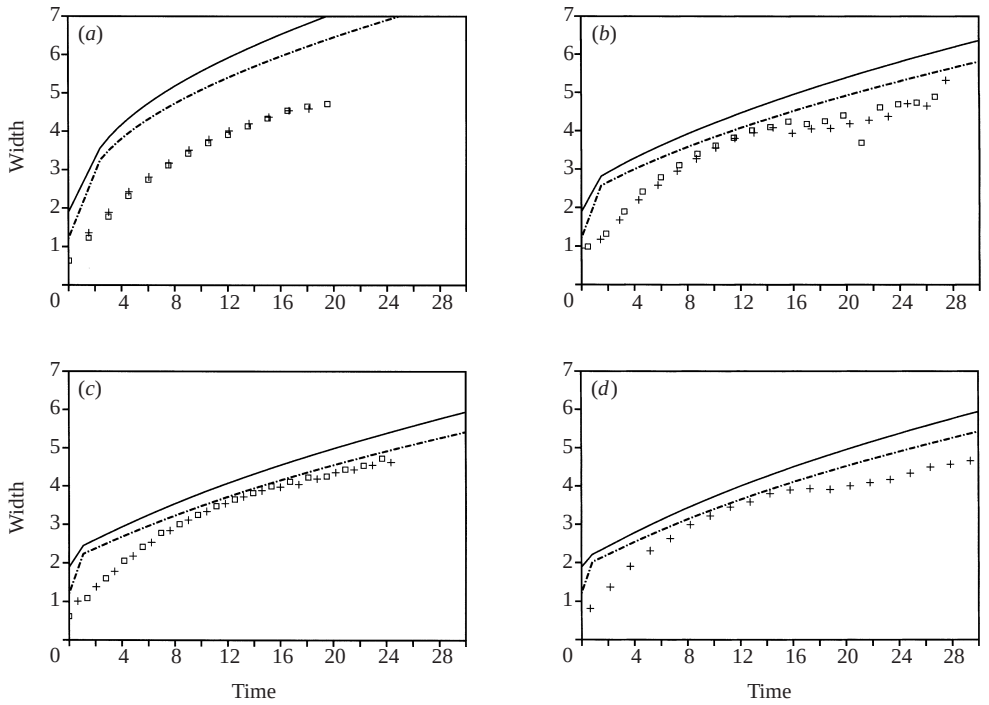

FIGURE 7. Width of the gravity current against time for slopes of (*a*) 5°, (*b*) 10°, (*c*) 15° and (*d*) 20°. +, □, experimental measurements; —, theoretical prediction of the wedge integral model in § 2 assuming the cylindrical wedge shape; – · –, prediction assuming the triangular wedge shape.

occur, possibly owing to the fact that vertical spreading is inhibited by the density difference between the current and the ambient. There is a relatively large error in the measurements of the height of the current owing to the fact that conductivity measurements were only taken at a discrete set of heights.

Figure 9 shows the maximum reduced gravity at the front of the current as a function of time. As can be seen in figures 10 and 11, the value fluctuates greatly within the head of the current. This fluctuation, combined with the discrete sampling time, means that there is a large fluctuation in the measured maximum value. The values do give some indication of the rate of dilution of the current. The wedge integral model assumes a uniform density distribution in the current rather than the value at the peak value at the front of the current, which explains why the experimental values are slightly higher than the integral model predictions. A better comparison would be using an experimentally determined, depth-integrated average density, rather than a peak density.

The reduced gravity profiles in figure 10 show that the current is divided into a relatively narrow but deep (≈ 4–6 cm) head region, with a much wider and shallower (≈ 1 cm) region behind where the fluid is slowly draining away. Viscous forces are likely to play a significant role in the shallower region. This is verified by the visual images of the flow in figure 3. The thicker crescent-shaped band of fluid which makes up the head is visible in the picture as a darker region, with a lighter thinner draining region behind it. The wedge integral model predicts a linear decrease in height from the maximum at the front to zero height at the back of the current. This does not agree precisely with the experiments.

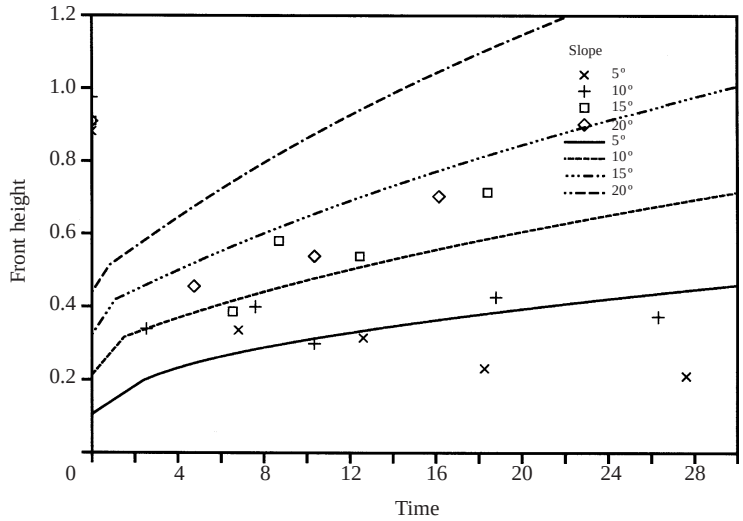

FIGURE 8. Height of the gravity current front against time for slopes of 5° to 20°. The symbols are measurements from experiments 12–18 made using the conductivity probe and the lines are the theoretical prediction of the wedge integral model in § 2.

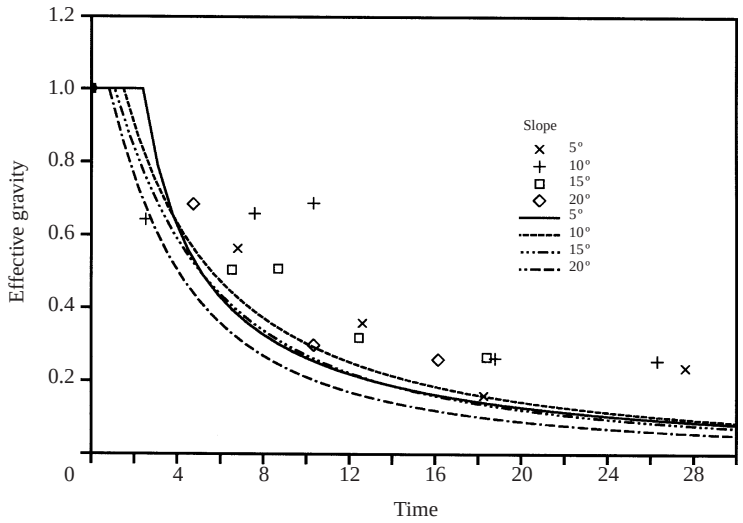

FIGURE 9. Reduced gravity of the gravity current front against time for slopes of 5°–20°. The points are experimental measurements and the lines are the theoretical prediction of the wedge integral model in § 2.

The intensity profile in figure 11 gives an indication of how the depth of the current changes as the current develops. The light intensity, I, is proportional to $\exp(-\int g' \, \mathrm{d}z)$ as described by Cenedese & Dalziel (1998). The vertically integrated g' is the pressure difference or head which is driving the gravity current forward. The values plotted are arbitrary units so that an increase in the plotted value corresponds to an increase in the head. It can be seen that as the current moves down the slope, the head is reduced slightly, which explains why the current slows down. The width of the head region can also be seen to increase as the current develops.

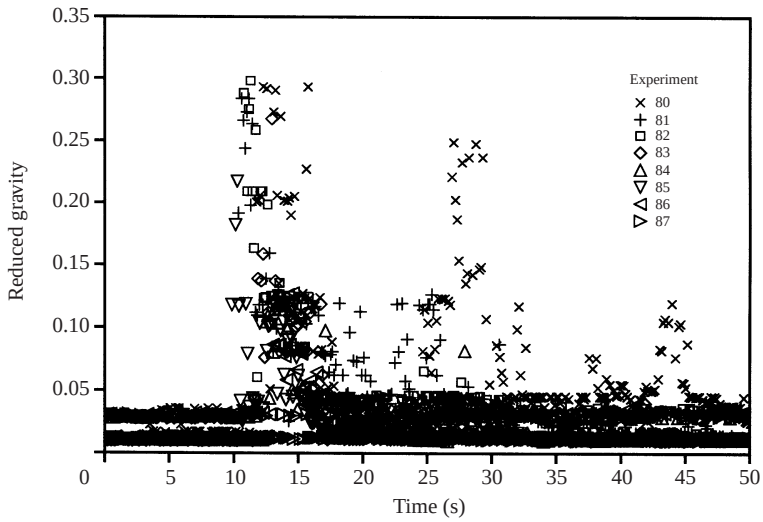

FIGURE 10. Reduced gravity against time at a series of different heights above the bottom. The slope is 15°.

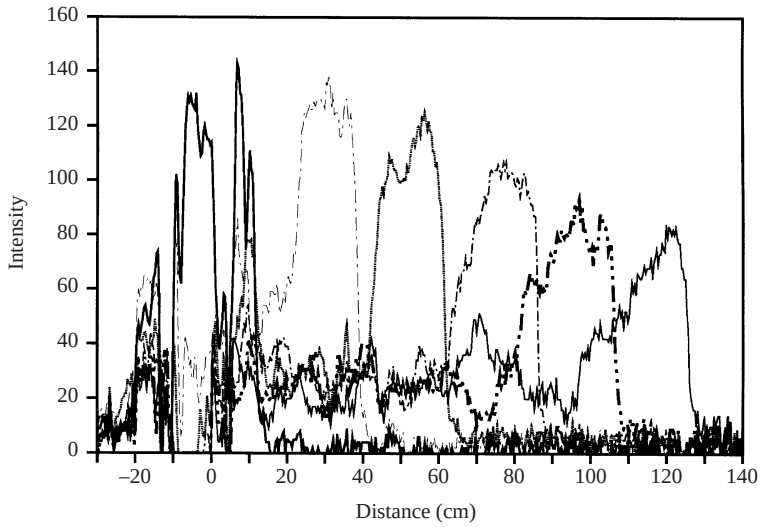

FIGURE 11. Centreline profiles of the light intensity at 3 s intervals showing the progress of the current down-slope and the development of the head. The intensity scale gives a measure of the vertical integral of g'. The experiment was on a slope of 15°.

The values for the entrainment coefficient, α, were obtained by doing a least-squares fit to the front position for each slope angle (see table 2). The values are averaged over all the experiments for each slope and are plotted in figure 12 as a function of slope angle and compared with other published values for similar situations. The entrainment is assumed to occur over a region at the front of the wedge with width comparable to the current height. This is the region where the majority of the fluid is and where it would be expected that the most mixing would occur. This is confirmed by the experiments described in § 4. In addition to the coefficients calculated from the experiments reported here, the graph includes the results from Beghin *et al.* (1981)

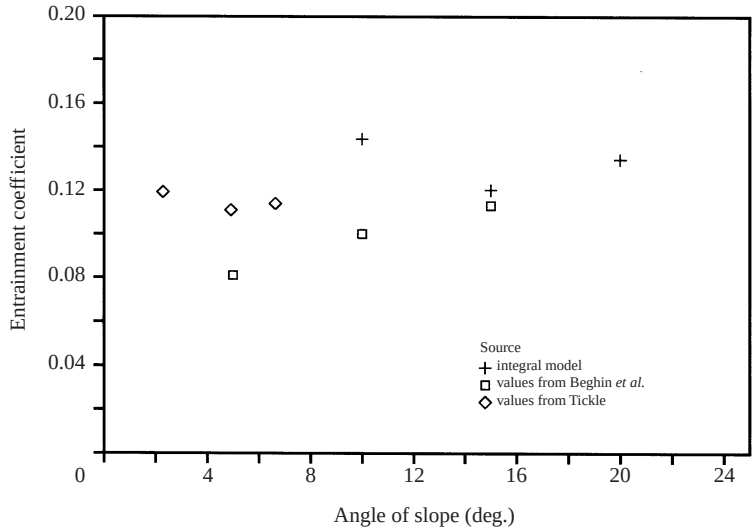

FIGURE 12. Comparison of entrainment coefficients as a function of slope from different experiments. +, best fit of current data to wedge integral model (cylindrical wedge); □, values from Beghin *et al.* (1981); ◇, values from Tickle (1996).

for a saline gravity current in a sloping channel and from Tickle (1996) for a three-dimensional release of dense gas on a slope. The values from Tickle (1996) agree well with the results here. The values from Beghin *et al.* (1981) also agree well, although they are on the whole slightly lower than the values for the three-dimensional gravity currents. In Beghin *et al.* (1981), the entrainment is assumed to occur over the whole head, so the slight difference in entrainment coefficient may be due to a difference in the area over which the entrainment is occurring. The entrainment coefficient is seen to be an approximately constant function of the slope. The work of Hallworth *et al.* (1996) for both two-dimensional and three-dimensional currents on a smooth horizontal surface, entraining over the whole head, gave values of between 0.08 and 0.09 for the entrainment coefficient, which agree with the results here for a gravity current on a slope. The results from Tickle (1996) were made assuming entrainment over the whole of the top of the wedge. Here, they are recalculated assuming the entrainment is limited to the head region. This assumption, which agrees with the experimental observations, removes most of the slope dependence seen by Tickle (1996) and Ellison & Turner (1959) in previous experiments. This suggests that for moderate slopes the fundamental entrainment processes may not be siginificantly different from those in a gravity current on a horizontal surface. Note that the value for 5° is significantly larger than the others (approximately 0.3). Study of the results for this experiment shows that the current is not reaching the assumed self-similar shape before reaching the edge of the tank, so it is not strictly appropriate to try and use this model to estimate the entrainment coefficient.

The Froude number of the gravity current front, $Fr = u_f/(g'_f h_f)^{1/2}$, was calculated for the experiments. The subscript f denotes the value of the variable at the front of the current. Figure 13 shows the results. One of the assumptions found in most models for gravity currents, including those of Webber *et al.* (1993) and Tickle (1996), is the assumption that the front Froude number is a constant. The wedge integral model does not include the constant-Froude-number assumption as an explicit condition. Instead, the drag on the current is included through the bottom drag coefficient, the

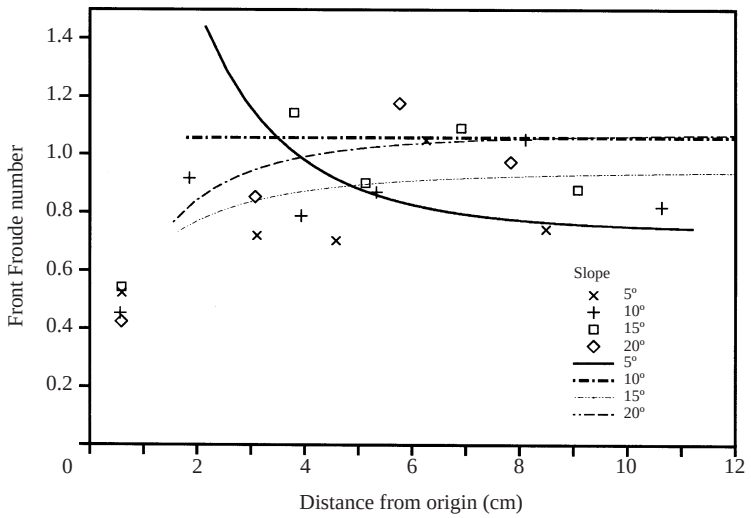

FIGURE 13. Froude numbers against down-slope distance for slopes of 5° to 20°. The symbols are experimental measurements and the lines are the theoretical predictions of the wedge integral model in § 2 assuming the cylindrical wedge shape.

added mass and the entrainment. The wedge integral model also predicts that the Froude number will tend to a constant value of

$$Fr \rightarrow \left(\frac{6S_3 \cos\theta}{\alpha S_4 (1 + C_A)(\gamma - 2)} \right)^{1/2}. \tag{4.1}$$

This value is a function of the slope as well as the parameters C_A, C_T, C_F and α. The dependence on the slope is very weak for moderate angles, θ, since $\cos\theta \approx 1$ for small θ and $\gamma - 2 \approx 4$ provided $\theta \gtrsim 5°$. Figure 13 shows that for a given experiment the Froude number remained constant to within about 20%, once the current was established. This is reasonable given that both the experimental front height and speed values are subject to an error of about 10%. The measured experimental values for the Froude number are in the range of 0.75–1.2, with a slight trend for the Froude number to increase with slope. This is comparable to the values for a gravity current on a flat bottom. Although the actual values predicted by the wedge integral model differ slightly, the general trends are the same. This all suggests that the assumption of constant Froude number used by Tickle (1996) may be reasonable. Experimental uncertainty in the measurements of the entrainment coefficient means that the ordering of the lines in figure 13 is not monotonic with slope.

The constant Froude number implies a constant Richardson number, $Ri = 1/Fr^2$. Work by Ellison & Turner (1959) showed that, provided the entrainment is through the top of the current head, the entrainment is a function of the Richardson number, so a constant Richardson number leads to a constant entrainment coefficient, as is assumed in the model and found from the experiments.

Viscous forces must be negligible for the models described here to be valid, i.e. the Reynolds number of the flow must be sufficiently large. The Reynolds number of the gravity current head is given by

$$Re = \frac{u_f h_f}{\nu} \tag{4.2}$$

where u_f and h_f are the front speed and height and ν is the kinematic viscosity. The

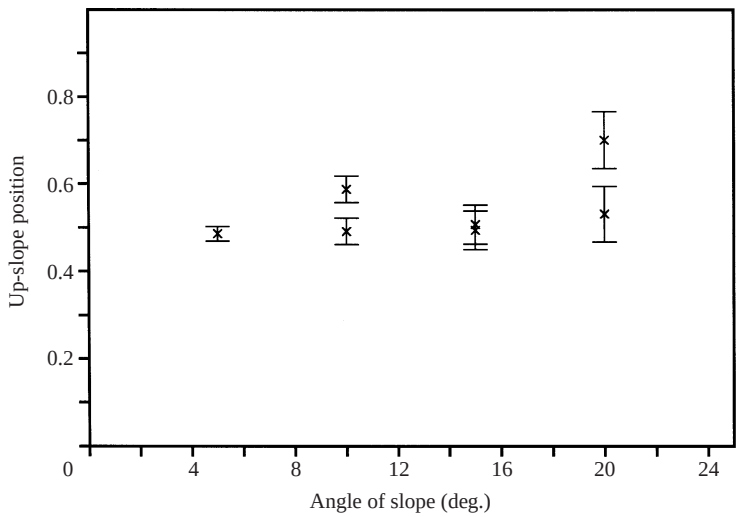

FIGURE 14. Maximum up-slope extent of the gravity current as a function of slope. The height is non-dimensionalized with respect to the initial height of the release.

Reynolds number varied slightly with the distance from the source. The minimum value for the experiments increased from around 1000 for the slope of 5° to about 7000 for the slope of 20°. In all cases, this is sufficient to allow the viscous effects to be neglected at the head. In the region behind the head, the Reynolds number is lower as the height is much less and the speed is also less. In the laboratory, viscous effects will always be important towards the rear of the wedge, but this does not appear to be important for driving the flow, at least until the viscous layer represents a significant fraction of the volume of the current. Eventually, the layer will have an effect, simply because there is much less fluid in the head.

The extent to which the current spreads up-slope is likely to be influenced by viscous forces, since the up-slope layer becomes thin and slow moving. Figure 14 shows the maximum up-slope extent as a function of the slope. The height to which the current rises is non-dimensionalized with the initial height of the release. It can be seen that the current rises to about half the initial height.

5. Conclusions

The experimental work reported here demonstrates that even for relatively gentle slopes, the presence of a sloping boundary can have a significant effect on a gravity current. Further, the role of entrainment is significant in slowing down the current as it flows down the slope.

Using the scaling in § 2.1, the time t_θ, given by (2.3), for the slope to become important is found.

Once the slope has become important, the gravity current develops into a wedge shape which moves down the slope. The similarity solution from the shallow-water model of Webber *et al.* (1993) does not accurately predict the motion of the gravity current, as it fails to take into account the entrainment of the ambient fluid into the current. The model of Tickle (1996) includes the entrainment in a simple manner, which leads to better prediction of the front position, but does not accurately capture the shape of the gravity current. In particular, the width is over-predicted and the

wedge is seen to have more of a triangular shape than the circular shape predicted by the shallow-water models.

The wedge integral model developed here is more successful than the non-entraining shallow-water model in predicting front position where slope effects are important. Neither type of model is valid for the initial stages of the flow where the slope can be neglected. For a suitable choice of the shape parameters in the integral model, a good fit to the current shape, width and length can be obtained. The model also provides a reasonable prediction of the reduced gravity of the current. The entrainment coefficient is found to be approximately constant, provided the entrainment is taken to occur in a region near the front of the gravity current of width comparable to the wedge height. Experimentally, this is the region where the most vigorous mixing is observed and where the bulk of the fluid is located. The values for the entrainment coefficient agree well with previous work in similar situations.

Both the experiments and the integral model suggest that, once the wedge-shaped gravity current has developed, the front Froude number is a constant of the flow, independent of time and slope. For an axisymmetric gravity current on a horizontal surface, this result is well known, but has not been reported previously for a sloping bottom.

The entraining wedge integral model does not predict all of the remaining details of the flow accurately. The shape of the gravity current observed in the laboratory is more complicated than the simple wedge shapes assumed by the models. In fact, it is more of a crescent shape and behind the crescent is a thin layer of draining fluid. Within this thin layer, viscous forces are likely to be important. This region is not included in any of the models discussed here. This may explain the tendency of both the entraining shallow-water model of Tickle (1996) and the wedge integral model to over-predict the width and length of the current when compared with the experiments. It appears that the bulk motion of the current is controlled by the front of the current, as for an axisymmetric current on a horizontal surface. Any integral model which predicts this part of the flow reasonably accurately with give a fair prediction for the bulk motion of the current. This helps to explain why the integral model does so well, despite not including many of the more complicated aspects of the flow.

For dense gas dispersion in the atmosphere, the draining region may be different as the dominant effect is likely to be turbulent diffusion rather than viscous diffusion. In addition, any wind will be important, but that is neglected here. We have shown that for smooth surfaces the bottom drag is not significant in determining the bulk motion of the current; however, for a rough surface, such as tall vegetation or buildings, the results may be affected by the bottom drag term. Nonetheless, the experimental data and wedge integral model presented here provide a useful check for more complicated existing and future dense gas dispersion models. The experiments demonstrate that the presence of a relatively gentle slope may have a large influence on the area affected by a spillage of dense gas and also on the dose received at a given point.

ANR was supported in this work by an EPSRC CASE studentship in conjunction with the HSE.

REFERENCES

Alavian, V. 1986 Behaviour of density currents on an incline. *J. Hydraul. Engng ASCE* **112**, 27–42.
Batchelor, G. 1967 *An Introduction to Fluid Dynamics*. Cambridge University Press.

Beghin, P., Hopfinger, E. & Britter, R. 1981 Gravitational convection from instantaneous sources on inclined planes. *J. Fluid Mech.* **107**, 407–422.

Bonnecaze, R. & Lister, J. 1999 Particle-driven gravity currents down planar slopes. *J. Fluid Mech.* **390**, 75–92.

Britter, R. & Linden, P. 1980 The motion of the front of a gravity current travelling down an incline. *J. Fluid Mech.* **99**, 531–543.

Cenedese, C. & Dalziel, S. 1998 Concentration and depth fields determined by the light transmitted through a dyed solution. In *Proceedings of the 8th International Symposium on Flow Visualization* (ed. C. Carlomagno & G. Grant).

Dade, W., Lister, J. & Huppert, H. 1994 Fine-sediment deposition from gravity surges on uniform slopes. *J. Sed. Res.* **A64**, 423–432.

Dalziel, S. 1992 *Digimage: System Overview*. Cambridge Environmental Research Consultants, Ltd.

Ellison, T. & Turner, J. 1959 Turbulent entrainment in stratified flow. *J. Fluid Mech.* **6**, 423–448.

Gröbelbauer, H., Fanneløp, T. & Britter, R. 1993 The propogation of intrusion fronts of high density ratio. *J. Fluid Mech.* **250**, 669–687.

Hallworth, M., Huppert, H., Phillips, J. & Sparks, S. 1996 Entrainment into two-dimensional and axisymmetric turbulent gravity currents. *J. Fluid Mech.* **308**, 289–311.

Huppert, H. & Simpson, J. 1980 The slumping of gravity currents. *J. Fluid Mech.* **99**, 785–799.

Huq, P. 1996 The role of aspect ratio on entrainment rates of instantaneous axisymmetric finite volume releases of dense fluid. *J. Haz. Mat.* **49**, 89–101.

Lister, J. 1992 Viscous flows down an inclined plane from point and line sources. *J. Fluid Mech.* **242**, 631–653.

Morton, B., Taylor, G. & Turner, J. 1956 Turbulent gravitational convection from maintained and instantaneous sources. *Proc. R. Soc. Lond.* A **234**, 1–23.

Simpson, J. 1997 *Gravity Currents in the Environment and the Laboratory*, 2nd edn. Cambridge University Press.

Tickle, G. 1996 A model of the motion and dilution of a heavy gas cloud released on a uniform slope in calm conditions. *J. Haz. Mat.* **49**, 29–47.

Tsihrintzis, V. & Alavian, V. 1996 Spreading of three-dimensional inclined gravity plumes. *J. Hydraul. Res.* **34**, 695–711.

Webber, D., Jones, S. & Martin, D. 1993 A model of the motion of a heavy gas cloud released on a uniform slope. *J. Haz. Mat.* **33**, 101–122.